Anomalous behavior in entanglement speed profile through spin chains

Fatemeh Sadeghi, Mostafa Motamedifar ⬤,* and Mojtaba Golshani ⬤

Faculty of Physics, Shahid Bahonar University of Kerman, Kerman 7616913439, Iran

The origin of the uniform Dzyaloshinskii-Moriya interaction (DMI), which is responsible for the creation of chiral magnetism, has been the subject of extensive research. Recently, modern technology has allowed for its production and utilization in a modulated form. Not only can magnetic phases of spin chains be enriched by the presence of such a potential as detailed in Japaridze *et al.* [Phys. Rev. E **104**, 014134 (2021)], but the capacity of such systems for information transmission is also greatly enhanced. The current paper examines the impact of a staggered pattern of DMI (STDMI) on a chain with a substrate XX Heisenberg interaction. It is demonstrated how enhancing the intensity of this coupling improves the propagation of an entangled quantum state. Additionally, as our analysis has shown, the initial condition over the system's state has a profound effect on the speed at which entanglement spreads. The aberrant behavior of the entanglement's speed profile in response to fine-tuning of the phase factor which adjusts the initial state is the focus of this paper. This anomalous behavior is characterized by dramatic drops in speed for certain phase factor values. We have also shown that, using wave interference principles, we can predict exactly why these phenomena occur. This research will pave the way for additional studies on STDMI and its potential applications in the field of quantum information.

I. INTRODUCTION

The dynamic evolution of many-body or statistical systems has long been a topic of interest in physics and other branches of science. If the number of particles in the system is very large, investigating the behavior of such a system with numerical approaches may lead to problems; in this case, having an exact solution is extremely valuable. In such systems, the emergence of a critical point at which the system behaves erratically has been of great importance to statistical mechanics researchers. In many circumstances, the system's anomalous behavior is triggered by the initial condition of the problem. The aforementioned systems are widely employed even in the realm of quantum information and computation.

In the present paper, we look at the dynamic evolution of a many-particle system employed in quantum information science, which has an anomalous behavior for the transmission of entanglement that is reliant on the initial conditions. By having an exact solution for the problem, we were able to get rid of the challenges arisen by approximate and numerical methods.

Quantum computing may be realized on a diversity of platforms, consisting of cold atoms [1,2], trapped ions [3–6], and superconducting quantum circuits [7–10]. On these platforms, controlling the transferring of quantum states is a foundational prerequisite. While quantum communication over long distances has been achieved to a long distance in free space and optical fibers [11–13], it is still crucial to create chances for transferring quantum states across solid-state equipment. A variety of quantum state transfer (QST) protocols for various solid-state instruments have been proposed [14–19]. There has been considerable interest in QST through the use of a spin chain in last years, and several methods have been developed for this purpose; see Refs. [20–22] just to name but a few.

The rich magnetic phases of a spin chain with Heisenberg-type magnetic interaction in many forms (such as the XY type [23–25], XXZ chain [26], or the compass model [27–30], for example) have recently attracted considerable interest. Such systems may also serve as a quantum data bus over practical distances, as proved by Bose in Ref. [31]. According to the proposal, a quantum state is encoded on a spin at one end of the chain to initiate communication, followed by a wait period at the other end. Spin chains have not been the only structures utilized to accomplish this objective; more intricate structures like honeycomb and two-leg ladders have also been implemented recently [32,33].

Aside from the Heisenberg interaction, another type of magnetic coupling, i.e., Dzyaloshinskii-Moriya interaction (DMI) has been thoroughly investigated in the field of entanglement dynamics research [34–36]. Historically, Dzyaloshinskii [37] and Moriya [38] introduced such an anisotropic antisymmetric interaction that results from the spin-orbit effect. Its initial application was an example of the antiferromagnetic interaction; however, Kavokin demonstrated that it also takes place on quantum dots [39]. The DMI was shown to be artificially sensitive to gating, voltage bias, and temperature difference between the dots, in addition to the spin polarization of the system, as demonstrated by Fransson *et al.* [40]. To observe the effect of DMI on the QST, we represent this interaction as an assist driving in the XX model described by the Hamiltonian

$$\mathcal{H} = \sum_j J\big(S_j^x S_{j+1}^x + S_j^y S_{j+1}^y\big) + \sum_j \mathbf{D}_j \cdot [\mathbf{S}_j \times \mathbf{S}_{j+1}], \quad (1)$$

where $\mathbf{D}_j$ is the DM vector along a preferred axis (generally corresponding to Heisenberg model $\hat{z}$ is preferable).

---

*Corresponding author: m.motamedifar@gmail.com

Symmetry limitations determined by the features of physical solid-state substances usually exclude the vast majority of alternatives and confine theoretical debate to two primary instances: uniform DMI [41–43] and staggered DMI [44–46], in which **D** is parallel on neighboring links for the former but antiparallel for the latter. We previously estimated the rate at which a QST occurs in a Heisenberg model with uniform DMI [47]. Then, we could wonder how the QST procedure differs, depending on whether the DMI is uniform or staggered. In the present paper, we report findings that particularly address how the staggered DMI affects QST. Not only does the obtained exact solution of the problem eliminate limitations imposed by the number of particles associated with the numerical tools but the mathematical method employed here may be lucrative for future research.

Because QST is believed to be associated with entanglement propagation [48,49], we employ entanglement notions to monitor the QST procedure. In fact, the current paper's central idea is to understand how the maximal entanglement that is initially shared by the first pair of the chain propagates over the remaining initially unentangled pairs. Whenever we refer to a chain, we are talking about the XX model modulated by STDMI.

We structured the paper as follows to deal with the aforementioned scenarios in detail: In Sec. II, we describe the XX chain with additional staggered DMI, along with the major steps of the analytic methodologies used to dynamically evolve the initial state of the system. Section III describes the entanglement measurement utilized in this paper. Section IV discusses the most impressive findings for entanglement propagation. Lastly, Sec. V summarizes the findings and conclusions.

II. DESCRIPTION OF THE MODEL AND TIME EVOLUTION OF THE INITIAL STATE

This section will examine the dynamic behavior of entanglement in a spin-1/2 chain modulated by the STDMI. For this purpose, we first introduce the Hamiltonian of the desired system, which is considered as follows:

$$\mathcal{H} = \sum_j J\left(S_j^x S_{j+1}^x + S_j^y S_{j+1}^y\right) + \sum_j (-1)^j \mathbf{D} \cdot [\mathbf{S}_j \times \mathbf{S}_{j+1}]. \tag{2}$$

The first term of Eq. (2) described the Heisenberg interaction via the XX model where S_j^x and S_j^y are respectively x and y component of spin operators on jth position. Moreover, the second one introduces the alternating DM coupling over the chain. This section assumes that **D** is oriented along the $\hat{z}$ axis of spin space, with the coordinates $\mathbf{D} = (0, 0, D)$. The symbol D represents the magnitude of STDMI's strength in all subsequent calculations. In addition, by employing Jordan-Wigner transformations,

$$S_j^+ = c_j^\dagger e^{i\pi \sum_{\ell<j} c_\ell^\dagger c_\ell}, \quad S_j^- = e^{-i\pi \sum_{\ell<j} c_\ell^\dagger c_\ell} c_j,$$
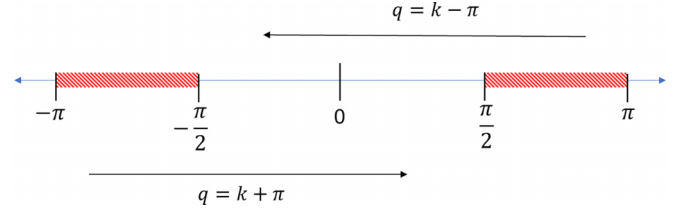
$$S_j^z = c_j^\dagger c_j - \frac{1}{2}.$$

FIG. 1. Schematic picture of moving into the reduced Brillouin zone and consequent changing variables [see Eq. (6)].

The earliest spin Hamiltonian is reconstructed in terms of spinless fermions as follows:

$$\begin{aligned}
H_f = &\sum_j \frac{J}{2}(c_j^\dagger c_{j+1} + c_{j+1}^\dagger c_j) \\
&+ \sum_j \frac{iD}{2} e^{ij\pi}(c_j^\dagger c_{j+1} - c_{j+1}^\dagger c_j),
\end{aligned} \tag{3}$$

where $c_j^\dagger$ (c_j) indicates the creation (annihilation) operator for spinless fermions at the jth site. Following the Fourier transformation,

$$c_j = \frac{1}{\sqrt{N}} \sum_k \tilde{c}_k e^{-ikj}, \tag{4}$$

the Hamiltonian is translated to Fourier language in the momentum space. Then the diagonalization process will be carried out there. As a result of calculations, the following result is obtained:

$$\begin{aligned}
\tilde{H} = &\sum_k [J\cos(k)\tilde{c}_k^\dagger \tilde{c}_k - iD\cos(k)\tilde{c}_k^\dagger \tilde{c}_{k+\pi}], \\
&k = \frac{2\pi j}{N} \quad j = -\frac{N}{2}, -\frac{N}{2} + 1, \ldots, \frac{N}{2} - 1,
\end{aligned} \tag{5}$$

where we take the lattice constant equal to unity ($a \equiv 1$). To implement the diagonalization process, we must restrict ourselves to the reduced Brillouin zone ($-\pi/2 \leqslant k < \pi/2$); see Fig. 1. For this purpose, we consider that

$$\sum_{-\pi \leqslant k < \pi} \bigcirc = \sum_{-\pi \leqslant k < -\pi/2} \bigcirc + \sum_{-\pi/2 \leqslant k < \pi/2} \bigcirc + \sum_{\pi/2 \leqslant k < \pi} \bigcirc.$$

Here, any term appeared in the front of the summation [Eq. (5)] is substituted by the circle symbol. For $-\pi \leqslant k < -\pi/2$, we can define $q = k + \pi$ so the previous interval moves into $[0, \pi/2)$ by the wave number of q. So, for $\pi/2 \leqslant k < \pi$, we choose $q = k - \pi$, then the last term of Eq. (6) goes into $q \in [-\pi/2, 0)$. Moreover, because the wave number of $\tilde{c}_{q+\pi}^\dagger$ differs by 2π from the wave number of $\tilde{c}_{q-\pi}^\dagger$, then they are equivalent. It makes that Eq. (5) can be cast into

$$\begin{aligned}
\tilde{H} = &\sum_{q=0}^{\pi/2} [-J\cos(q)\tilde{c}_{q+\pi}^\dagger \tilde{c}_{q+\pi} + iD\cos(q)\tilde{c}_{q+\pi}^\dagger \tilde{c}_q] \\
&+ \sum_{q=-\pi/2}^{\pi/2} [J\cos(q)\tilde{c}_q^\dagger \tilde{c}_q - iD\cos(q)\tilde{c}_q^\dagger \tilde{c}_{q+\pi}] \\
&+ \sum_{q=-\pi/2}^{0} [-J\cos(q)\tilde{c}_{q+\pi}^\dagger \tilde{c}_{q+\pi} + iD\cos(q)\tilde{c}_{q+\pi}^\dagger \tilde{c}_q]. \tag{6}
\end{aligned}$$

The combination of the first and last term of Eq. (6) results in

$$\tilde{H} = \sum_{q=-\pi/2}^{\pi/2} [-J\cos(q)\tilde{c}_{q+\pi}^\dagger \tilde{c}_{q+\pi} + iD\cos(q)\tilde{c}_{q+\pi}^\dagger \tilde{c}_q]$$

$$+ \sum_{q=-\pi/2}^{\pi/2} [J\cos(q)\tilde{c}_q^\dagger \tilde{c}_q - iD\cos(q)\tilde{c}_q^\dagger \tilde{c}_{q+\pi}]. \quad (7)$$

By introducing $\tilde{c}_{q+\pi} = \tilde{d}_q^\dagger$, the final form of the Hamiltonian is summarized as follows:

$$\tilde{H} = \sum_q [J\cos(q)(\tilde{c}_q^\dagger \tilde{c}_q - \tilde{d}_q^\dagger \tilde{d}_q) - iD\cos(q)(\tilde{c}_q^\dagger \tilde{d}_q - \tilde{d}_q^\dagger \tilde{c}_q)]. \quad (8)$$

According to the goal of the problem, which is to investigate the propagation of entanglement in a spin chain over time, we need an initial entangled state between two arbitrary neighbors and then the effect of the time evolution operator on it. To this end, we consider an initial state as Eq. (9), where N counts system's particles. Moreover, φ is a phase factor and $|0\rangle$ and $|1\rangle$ refer to the eigenstates of the z component of the spin operator such that $S^z|0\rangle = -\hbar/2|0\rangle$ and $S^z|1\rangle = \hbar/2|1\rangle$:

$$|\psi(t=0)\rangle = \frac{|1_A 0_B\rangle + e^{i\varphi}|0_A 1_B\rangle}{\sqrt{2}} \otimes \underbrace{|00...0\rangle}_{N-2}. \quad (9)$$

As long as the system is subject to the unitary dynamics as a result of the time evolution operator $\hat{U}(t) = \exp(-i\hat{H}t/\hbar)$,

we would like to express its application to the initial state as

$$\hat{U}(t)|\psi(0)\rangle = \exp\left\{\frac{-iJt}{\hbar}\left[\sum_q \cos(q)(\tilde{c}_q^\dagger \tilde{c}_q - \tilde{d}_q^\dagger \tilde{d}_q)\right. \right.$$

$$\left.\left. -i\frac{D}{J}\cos(q)(\tilde{c}_q^\dagger \tilde{d}_q - \tilde{d}_q^\dagger \tilde{c}_q)\right]\right\}|\psi(0)\rangle, \quad (10)$$

where $|\psi(0)\rangle = \frac{1}{\sqrt{2}}(c_A^\dagger + e^{i\varphi}c_B^\dagger)|0\rangle$. Considering Eq. (10), t and D are then normalized to $\hbar/J$ and J, respectively. Then, in this situation, we assume $\hbar \equiv 1$ and $|J| = 1$ without sacrificing generality. As a result, t and D get to be dimensionless parameters in the following computations.

Even if we did our work here at zero temperature and for a closed system, the desired method may also be tested in a scenario of equilibrium [50] or in the presence of a heat source with a temperature of T by defining the memory [51] and the absence of that [52].

In the case of using relation (8), we must use a modified Fourier transformation of fermionic creation or annihilation operators in the reduced space:

$$c_j^\dagger = \frac{1}{\sqrt{N}} \sum_{\frac{-\pi}{2} \leqslant q < \frac{\pi}{2}} (\tilde{d}_q^\dagger e^{i(q+\pi)j} + \tilde{c}_q^\dagger e^{iqj}). \quad (11)$$

With the combination of two Eqs. (9) and (10) in addition to using Eq. (11), we have

$$|\psi(t)\rangle = \frac{e^{-it\tilde{H}}}{\sqrt{2N}}\left(\underbrace{\sum_q e^{iq}\tilde{c}_q^\dagger + e^{i(q+\pi)}\tilde{d}_q^\dagger}_{c_A^\dagger} + e^{i\varphi}\underbrace{\sum_q e^{2iq}\tilde{c}_q^\dagger + e^{2i(q+\pi)}\tilde{d}_q^\dagger}_{c_B^\dagger}\right)|0\rangle$$

$$= \frac{e^{-it\tilde{H}}}{\sqrt{2N}}\sum_q [(e^{iq} + e^{2iq+i\varphi})\tilde{c}_q^\dagger - (e^{iq} - e^{2iq+i\varphi})\tilde{d}_q^\dagger]|0\rangle. \quad (12)$$

To apply the time evolution operator, we must diagonalize the considered Hamiltonian through which we use a unitary operator as

$$\mathcal{U} = \begin{pmatrix} \cos(\alpha) & i\sin(\alpha) \\ i\sin(\alpha) & \cos(\alpha) \end{pmatrix}, \quad (13)$$

where

$$\alpha = \arctan\left(\frac{J - \sqrt{J^2 + D^2}}{D}\right). \quad (14)$$

In other words, the Hamiltonian (8) can be diagonalized with a new basis:

$$\tilde{\gamma}_q^\dagger = \cos(\alpha)\tilde{c}_q^\dagger + i\sin(\alpha)\tilde{d}_q^\dagger, \quad \tilde{\beta}_q^\dagger = i\sin(\alpha)\tilde{c}_q^\dagger + \cos(\alpha)\tilde{d}_q^\dagger. \quad (15)$$

Then, the result of $\mathcal{U}^\dagger \tilde{H} \mathcal{U}$ yields diagonalized Hamiltonian in the same basis:

$$\tilde{H} = \sum_q (\underbrace{\sqrt{J^2 + D^2}\cos(q)}_{\varepsilon(q)})[\tilde{\gamma}_q^\dagger \tilde{\gamma}_q - \tilde{\beta}_q^\dagger \tilde{\beta}_q]. \quad (16)$$

Based on Eqs. (12) and (15), we have

$$|\psi(t)\rangle = \frac{e^{-it\tilde{H}}}{\sqrt{2N}}\sum_q \left[\underbrace{(e^{iq+i\alpha} + e^{i\varphi}e^{2iq-i\alpha})}_{\eta(q)}\tilde{\gamma}_q^\dagger + \underbrace{(e^{i\varphi}e^{2iq-i\alpha} - e^{iq+i\alpha})}_{\zeta(q)}\tilde{\beta}_q^\dagger\right]|0\rangle. \quad (17)$$

In other words,

$$|\psi(t)\rangle = \frac{e^{-it\sum_{k'}\varepsilon(k')[\tilde{\gamma}_{k'}^\dagger\tilde{\gamma}_{k'}-\tilde{\beta}_{k'}^\dagger\tilde{\beta}_{k'}]}}{\sqrt{2N}}\sum_q[\eta(q)\tilde{\gamma}_q^\dagger+\zeta(q)\tilde{\beta}_q^\dagger]|0\rangle. \tag{18}$$

To apply the time evolution operator, we must expand it as

$$|\psi(t)\rangle = \frac{1}{\sqrt{2N}}\sum_q\left\{1-it\sum_{k'}\varepsilon(k')[\tilde{\gamma}_{k'}^\dagger\tilde{\gamma}_{k'}-\tilde{\beta}_{k'}^\dagger\tilde{\beta}_{k'}]+\frac{(-it)^2}{2!}\left(\sum_{k'}\varepsilon(k')[\tilde{\gamma}_{k'}^\dagger\tilde{\gamma}_{k'}-\tilde{\beta}_{k'}^\dagger\tilde{\beta}_{k'}]\right)^2+\cdots\right\}(\eta(q)\tilde{\gamma}_q^\dagger+\zeta(q)\tilde{\beta}_q^\dagger)|0\rangle. \tag{19}$$

Considering the anticommutator relations $\{\tilde{\gamma}_q^\dagger,\tilde{\gamma}_{k'}\}=\{\tilde{\beta}_q^\dagger,\tilde{\beta}_{k'}\}=\delta_{qk}$, $\{\tilde{\gamma}_q^\dagger,\tilde{\beta}_q\}=\{\tilde{\gamma}_q,\tilde{\beta}_q^\dagger\}=0$, we get $\tilde{\gamma}_{k'}^\dagger\tilde{\gamma}_{k'}\tilde{\gamma}_q^\dagger|0\rangle=\delta_{k'q}\tilde{\gamma}_q^\dagger|0\rangle$ and $\tilde{\beta}_{k'}^\dagger\tilde{\beta}_{k'}\tilde{\beta}_q^\dagger|0\rangle=\delta_{k'q}\tilde{\beta}_q^\dagger|0\rangle$. For this reason,

$$|\psi(t)\rangle = \frac{1}{\sqrt{2N}}\sum_q\eta(q)\underbrace{\left(1-it\varepsilon(q)+\frac{1}{2!}(-it\varepsilon(q))^2+\cdots\right)}_{e^{-it\varepsilon(q)}}\tilde{\gamma}_q^\dagger|0\rangle+\frac{1}{\sqrt{2N}}\sum_q\zeta(q)\underbrace{\left(1+it\varepsilon(q))+\frac{1}{2!}(it\varepsilon(q))^2+\cdots\right)}_{e^{it\varepsilon(q)}}\tilde{\beta}_q^\dagger|0\rangle. \tag{20}$$

Because we intend to employ $c_j^\dagger$ again acting on $|0\rangle$, we must return to the old basis by utilizing Eq. (15) in an inverse process. Moreover, considering $\varepsilon(q)=\tilde{J}\cos(q)$ where $\tilde{J}=\sqrt{J^2+D^2}$, we reach

$$|\psi(t)\rangle = \frac{1}{\sqrt{2N}}\sum_q\sum_l(-i)^l\eta(q)\mathcal{J}_l(\tilde{J}t)e^{iql}\cos(\alpha)\tilde{c}_q^\dagger|0\rangle+\frac{1}{\sqrt{2N}}\sum_q\sum_l(-i)^l\eta(q)\mathcal{J}_l(\tilde{J}t)e^{iql}i\sin(\alpha)\tilde{d}_q^\dagger|0\rangle$$

$$+\frac{1}{\sqrt{2N}}\sum_q\sum_l(i)^l\zeta(q)\mathcal{J}_l(\tilde{J}t)e^{iql}i\sin(\alpha)\tilde{c}_q^\dagger|0\rangle+\frac{1}{\sqrt{2N}}\sum_q\sum_l(i)^l\zeta(q)\mathcal{J}_l(\tilde{J}t)e^{iql}\cos(\alpha)\tilde{d}_q^\dagger|0\rangle, \tag{21}$$

where $\mathcal{J}_s$ denotes the Bessel function of the first order s [53]. In the next step, by modifying the variable $\kappa=q+\pi$ in the last term of Eq. (21) and the variable names $(q\rightarrow\kappa)$ in the first expression, we find that the first and last ones of this equation can be concatenated in such a way as to cover the range 0 to 2π. The second and third terms follow the same procedure. Consequently, we can write

$$|\psi(t)\rangle = \frac{1}{\sqrt{2N}}\sum_{\kappa,l}[(-i)^l(e^{i(2\kappa-\alpha)+i\varphi}+e^{i(\kappa+\alpha)})\cos(\alpha)+i^{l+1}(e^{i(2\kappa-\alpha)+i\varphi}-e^{i(\kappa+\alpha)})\sin(\alpha)]\mathcal{J}_l(\tilde{J}t)e^{i\kappa l}\tilde{c}_\kappa^\dagger|0\rangle. \tag{22}$$

Given that $\tilde{c}_\kappa^\dagger=\frac{1}{\sqrt{N}}\sum_j e^{-i\kappa j}c_j^\dagger$ and $\frac{1}{N}\sum_\kappa e^{-i(m-n)\kappa}=\delta_{m,n}$, we have

$$|\psi(t)\rangle = \sum_j a_j(t)c_j^\dagger|0..00\rangle,$$

$$a_j(t) = \frac{(-i)^{j-1}e^{i\alpha(1+(-1)^j)}}{\sqrt{2}}(\mathcal{J}_{j-1}(\tilde{J}t)+ie^{i(\varphi-2\alpha)}\mathcal{J}_{j-2}(\tilde{J}t)). \tag{23}$$

Here, $a_j(t)$ defines an amplitude, the magnitude of which indicates how probably a fermion occupies jth position in the chain. Then, we can see that Eq. (23) implements the single-particle states $(c_j^\dagger|00..0\rangle)$ to present each qubit's contribution to the time evolution of the wave function. This equation is crucial for calculating the system's density matrix to access a popular entanglement measurement, i.e., concurrence, for keeping an eye on the QST procedure in the following sections.

III. CONCURRENCE MONITORS QST

A system is said to be entangled if the quantum states of any two or more particles inside it are inextricably connected, even at great separations in space. In other words, once the particles in a system are in a superposition state, their quantum states are called to be entangled. One example of occurring entangled states is in the bipartite systems which have gained a lot of attention and interest. Such systems are made up of two components, for example, *A* and *B* which may be pure or mixed, and belong to a Hilbert space *H* of dimension *d*. Numerous notable approaches for characterizing and quantifying the measure of entanglement for such systems have been proposed. Bennett's entanglement of formation (E_f) [54] may be the most significant entanglement measure for bipartite systems. The von Neumann entropy $[S=-\text{Tr}\,\rho(\text{Log}\,\rho)]$ of the reduced density matrix $\rho=\rho_A(\rho_B)$ generated by partially tracing $\rho=|\Phi\rangle\langle\Phi|$ through one subsystem $B(A)$ is defined as the E_f for a pure state. Reference [55] is a good source that goes over the history and details of the entropy's concept. Now the question arises whether it is possible to define and calculate E_f for a mixed state as well. The answer of this question is positive. The E_f for a mixed state is then calculated by minimizing the E_fs associated with each pure state that contributes to the mixed state,

$$E_f(\rho) = \min\left\{\sum_i p_i E_f(\phi_i)\right\}, \tag{24}$$

in which ρ is the density matrix of a bipartite mixed state that defined as an ensemble of pure states as

$$\rho = \sum_i p_i |\phi_i\rangle\langle\phi_i|, \tag{25}$$

where $p_i \geqslant 0$ and $\sum_i p_i = 1$. The scenario of mixed states greatly complicates analytical processing of the extremization problem. Nevertheless, Hill and Wootters introduced the concurrence ($\mathcal{C}$) as an ancillary measure of E_f where A and B are two-level systems, such as a pair of qubits [56]. These two measures (E_f and $\mathcal{C}$) are related via the binary entropy (h) as $E_f = h(\frac{1}{2}[1 + \sqrt{1 - \mathcal{C}^2}])$, however, $\mathcal{C}$ almost can be considered a stand-alone measure of entanglement. In this relation, h acts on a variable, for example, x as $h(x) = -x \log_2(x) - (1 - x) \log_2(1 - x)$. For mixed states, the minimal average concurrences of pure states are given by [57]

$$\mathcal{C}(\rho) = \min \left\{ \sum_i p_i \mathcal{C}(\varphi_i) \right\}, \tag{26}$$

which is the modification of Eq. (24). Wootters derived the following straightforward expression for this minimization:

$$\mathcal{C}(\rho) = \max\{\lambda_1 - \lambda_2 - \lambda_3 - \lambda_4, 0\}, \tag{27}$$

where λ_js are the square roots of the eigenvalues of matrix $\mathcal{R} = \rho.(\sigma_y \otimes \sigma_y).\rho^*.(\sigma_y \otimes \sigma_y)$ that are decreasingly sorted. Here, $\rho(\rho^*)$ is the density matrix for a certain pair (conjugate of it) and σ_y is the y-component Pauli matrix. The concurrence varies from 0, indicating an unentangled state, to 1, representing a maximally entangled state. Due to the time-dependent nature of the quantum state, the concurrence function and the density matrix are likewise subject to temporal variation. To create a concurrence function between two particles in a multiparticle system, we should utilize the reduced density matrix (ρ_{mn}) obtained by tracing over all sites except for sites m and n (Ref. [58]). Moreover, the matrix form of ρ_{mn} against the two-point correlations between any two sites (m, n) can be expressed as follows:

$$\rho_{mn} = \frac{1}{4} \begin{pmatrix} \langle \mathscr{G}_m^\uparrow \mathscr{G}_n^\uparrow \rangle & \langle \mathscr{G}_m^\uparrow \sigma_n^- \rangle & \langle \sigma_m^- \mathscr{G}_n^\uparrow \rangle & \langle \sigma_m^- \sigma_n^- \rangle \\ \langle \mathscr{G}_m^\uparrow \sigma_n^+ \rangle & \langle \mathscr{G}_m^\uparrow \mathscr{G}_n^\downarrow \rangle & \langle \sigma_m^- \sigma_n^+ \rangle & \langle \sigma_m^- \mathscr{G}_n^\downarrow \rangle \\ \langle \sigma_m^+ \mathscr{G}_n^\uparrow \rangle & \langle \sigma_m^+ \sigma_n^- \rangle & \langle \mathscr{G}_m^\downarrow \mathscr{G}_n^\uparrow \rangle & \langle \mathscr{G}_m^\downarrow \sigma_n^- \rangle \\ \langle \sigma_m^+ \sigma_n^+ \rangle & \langle \sigma_m^+ \mathscr{G}_n^\downarrow \rangle & \langle \mathscr{G}_m^\downarrow \sigma_n^+ \rangle & \langle \mathscr{G}_m^\downarrow \mathscr{G}_n^\downarrow \rangle \end{pmatrix}, \tag{28}$$

where $\mathscr{G}_i^\uparrow = \mathbb{1} + \sigma^z$ and $\mathscr{G}_i^\downarrow = \mathbb{1} - \sigma^z$. Moreover, $\sigma^\pm = \sigma^x \pm i\sigma^y$. In Eq. (28), $\langle\rangle$ stands for the expectation values of any operator defined over the quantum state described by Eq. (23). For the system under consideration, concurrence between nearest neighbors can be summarized in the subsequent closed form

$$\mathcal{C}(\rho) = \sqrt{\Gamma_m \Gamma_{m+1}}, \tag{29}$$

in that

$$\Gamma_m = |\mathcal{J}_{m-1}(\sqrt{1 + D^2}t)|^2 + |\mathcal{J}_{m-2}(\sqrt{1 + D^2}t)|^2$$
$$- 2\mathcal{J}_{m-1}(\sqrt{1 + D^2}t)\mathcal{J}_{m-2}(\sqrt{1 + D^2}t)$$
$$\times \frac{\sin(\varphi)\mathrm{sgn}[J] + D\cos(\varphi)}{\sqrt{1 + D^2}}. \tag{30}$$

In Eq. (30), the function of sgn[.] determines the sign of J and since the value of $|J| = 1$, this function takes ± 1. In the present paper, we are interested in learning how entanglement is transmitted through the chain, hence we are measuring how much entanglement there is between the nearest of sites. In other words, we investigate the process of entanglement propagation between pairs of physically adjacent qubits. In the context of time evolution of concurrence, aspects of entanglement transmission are made available, such as its speed or its dependency on the phase factor. In the following section, we get into the essentials of it all.

IV. RESULTS

This section showcases the results attained for $\mathcal{C}$ and V (the speed of entanglement propagation) through the examination of several parameters and variables. Let us commence with Fig. 2, where panels (a)–(e) display the temporal evolution of $\mathcal{C}$ for distinct couples (where D and J are specified on each panel). To obtain these plots, we set φ equal to π, as will be discussed later. It is evident from the behavior of $\mathcal{C}$ in each panel that the maximum value of this function decreases as the distance between a typical pair (of qubits) and the initially entangled pair (IEP) increases. Moreover, by comparing Figs. 2(a)–2(e), it is evident that as D increases, the duration of the maximum value of $\mathcal{C}$ ($\mathcal{C}_{\max}$) decreases, i.e., the curves of concurrences become more compact. This compression exhibits that the transmission of the utmost degree of entanglement to the far qubits is accomplished in a reduced timeframe. In qualitative terms, this signifies that the transfer of entanglement has occurred at a faster rate. This is true for both ferromagnetism with $J < 0$ and antiferromagnetism with $J > 0$. Given Eq. (30), $\sin(\varphi = \pi) = 0$ (for plots of Fig. 2), it can be concluded that the sign of J does not influence the behavior of $\mathcal{C}$. Consequently, quantitative analysis also shows that the higher values of D result in a faster entanglement rate, as we will discuss below.

Here, we designate with X the distance between a typical pair ($j, j + 1$) and the IEP for the purpose of quantitatively calculating entanglement speed (V). The rate at which entanglement spreads is determined by the gradient of X against t. The speed, denoted by the symbol V without any subscripts, quantifies the rate at which entanglement is being transferred. Velocity, on the other hand, quantifies both the speed and direction of its movement. The speed refers to the absolute value of the velocity, meaning it is always positive and cannot be negative. The terms velocity and speed are often used interchangeably in daily conversation but they hold distinct meanings in the field of physics. In the present paper, it is employed of "speed" by focus on the magnitude of velocity.

As an illustration of speed calculation, we address the value of X which is equal to 1 for the pair (2,3), and equal to 2 for the pair (3,4), and so forth. Subsequently, we determine the specific time instance ($t_{\max}$) associated with the highest level of entanglement (represented by $\mathcal{C}_{\max}$) for each X. As a result, the variable X is graphed in Fig. 2(f) as a function of $t_{\max}$ for different values of D. For a given value of D, this panel demonstrates that the time interval between consecutive peaks remains constant, of course, by avoiding the critical condition that will be explained below. Then V can be defined as the
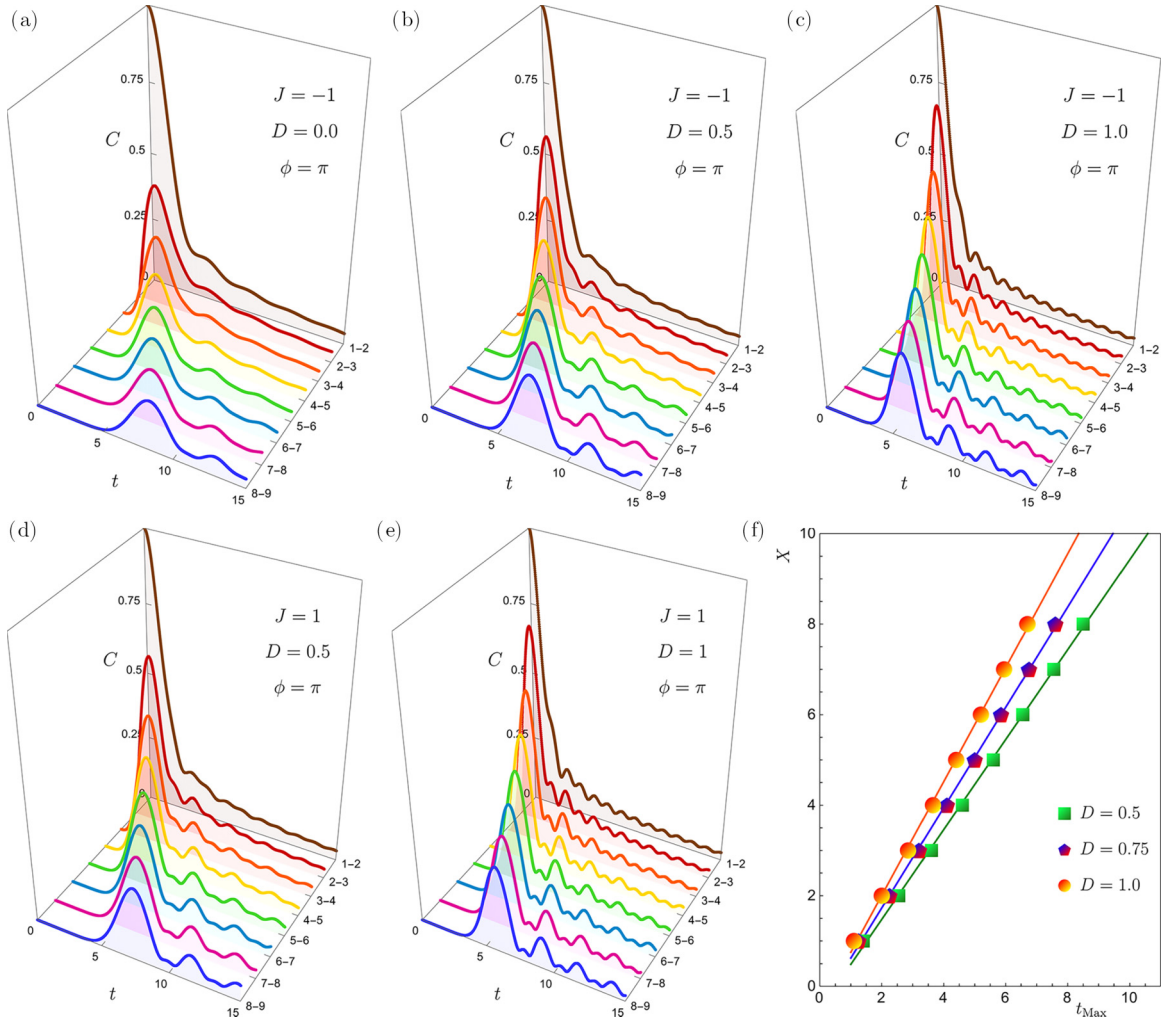
FIG. 2. (a)–(e) The behavior of concurrence towards time t for different pairs. Additionally, by comparing these figures we can see the effect of increasing value of staggered DMI. The first three are related to $J < 0$ and the next two are related to $J > 0$. For all plots, $\varphi = \pi$. As D increases, the concurrence's maxima happens in shorter time instances for any pairs showing V grows. (f) $X - t_{\max}$ dependency for different D values.

slope of the fitted lines. This is analogous to the position-time graphs of objects moving at a constant speed in Newtonian physics. These curves also illustrate that the speed of entanglement propagation improves as the value of D increases.

Nevertheless, the growth of the speed is not directly proportional to D, i.e., doubling D does not double the speed due to two main factors: first, the nature of $\tilde{J}$ in Eq. (23), which is determined by the value of D as $\tilde{J} = \sqrt{1 + D^2}$; second, the complex nature of mixing the value of J and D by the multiplication of $\sin(\varphi)$ and $\cos(\varphi)$ functions in the coefficient that appeared in Eq. (30).

Another notable fact that can be deduced from the comparison of Fig. 2(a) to Fig. 2(e) is that the peaks of concurrence for different pairs increase as the value of D increases, and this remains consistent for both ferromagnetic and antiferromagnetic conditions. However, this statement is not universally valid for any given value of φ. The increase in transmission speed is proportional to the growth of D. However, the extent to which $\mathcal{C}_{\max}$ varies in reaction to the growth of D depends entirely on the value of φ. For these specific figures, when the

value of φ is equal to π, a rise in D leads to a simultaneous enlargement of the peaks. On the other hand, when the value of D is increased at $\varphi = 0$, it leads to a decrease in the amount of peaks. We will discuss this topic again once we have clarified the meaning of Fig. 5.

Hence, it is vital to think about how the initial state's phase factor (φ) affects the behavior of entanglement transmission. The relevance of this parameter for the concurrence function is given by Eq. (30). The mysterious role that this parameter plays in the entanglement propagation process is illustrated in the plots of Fig. 3. For accessing these plots, fine adjustments were made to φ, and V was measured against the new settings. The top row of the corresponding figure, where $D = 1$, indicates that for a range of phase factors between $-\pi$ and 0, V drops considerably in the situation of $J = -1$. On the other hand, when J is positive, we observe that V also exhibits the same spectacular trend, of course, in $\varphi \in [0, \pi]$. To examine the impact of adjusting the value of D on both V and the critical interval, we put together the bottom row of Fig. 3. Regarding these two figures in this row, D is assigned a value
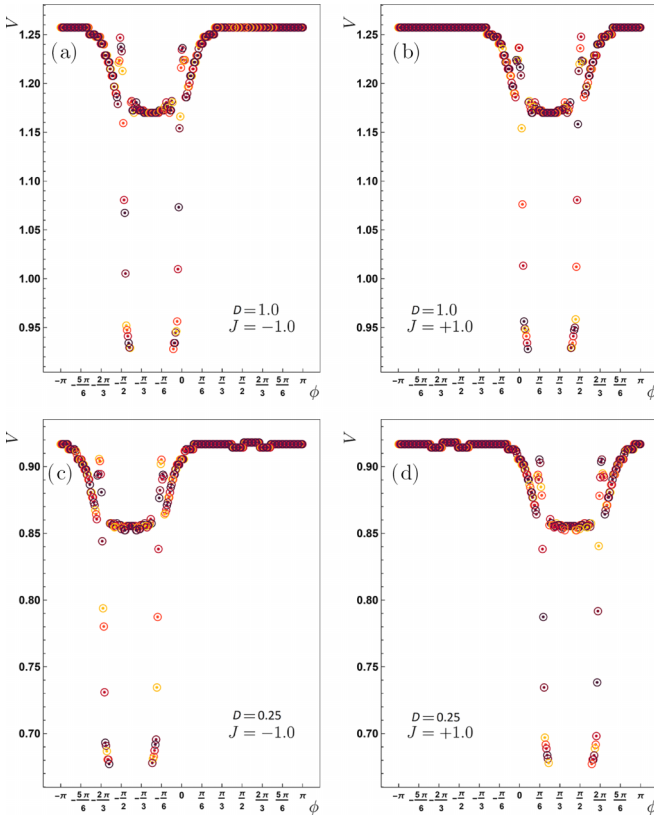
FIG. 3. The speed profile towards the phase factor is shown here. There are regions of φ in the speed profile where the value of V declines precipitously; this corresponds to the destructive interference of the waves in the context of wave interference. Beyond that specific region, the speed maintains a nearly constant value. Furthermore, the critical region of speed is observed for the ferromagnetic state in (a) and (c) when $\varphi < 0$, whereas it is defined for the antiferromagnetic state in (b) and (d) when $\varphi > 0$. Additionally, these plots illustrate that the speed does not diminish by the same magnitude when the power of D is reduced by a quarter for (c) and (d), compared to (a) and (b) (where its value is equal to one). Through the same comparison, it becomes evident that the critical region shifts further away from $\varphi = 0$ as the value of D decreases.

of 0.25. The comparison between the top and the bottom row of Fig. 3 confirms that as D decreases, not only does the speed value decrease but the position of the crucial zone also moves further away from $\varphi = 0$. The rationale behind this will subsequently be thoroughly elucidated.

We temporarily revisit Fig. 2 once more. As shown in its plots, each pair has a maximum value of concurrence ($\mathcal{C}_{max}$) at a specified time. The question here is how this maximum value is affected by the phase factor (φ). Figures 4(a) and 4(b) address this question. Although these plots show the results dedicated only to one particular pair (2,3), they are still applicable to other couples. As shown in these plots, when D is held constant ($D = 1$) and $J = -1$ or $J = +1$, the maximal value of $\mathcal{C}_{23}$ changes by tuning the value of φ.

To create Fig. 4(a) with $J < 0$, we first selected the value of $\pi/2$ for φ. Then, by modifying φ to $-\pi/2$, we can observe how the maximal value of $\mathcal{C}_{23}$ will decrease in this instance. In contrast, to produce Fig. 4(b) with $J > 0$, we initially chose
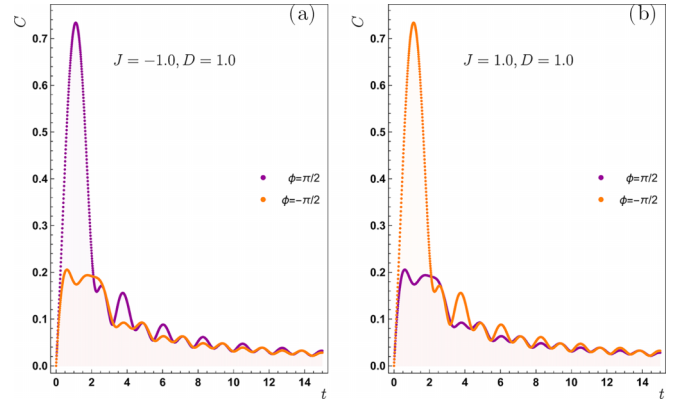

FIG. 4. To directly observe the effect of φ on the reduction of $\mathcal{C}_{max}$, the graphs of (a) are for $J < 0$ where concurrence between a typical pair (2,3) experiences a reduction when φ changes from $\pi/2$ to $-\pi/2$ and the graphs in (b) pertain to the case where $J > 0$, where concurrence between the considered pair decreases significantly as φ varies from $-\pi/2$ to $\pi/2$.

the value of $-\pi/2$ for φ. Subsequently, by adjusting it to $\pi/2$, we may analyze the corresponding reduction of $\mathcal{C}_{23}$ in this particular case. The selected values for φ precisely correspond to those provided in the speed profile depicted in Figs. 3. This implies that whenever $\mathcal{C}_{max}$ drops, we may experience a drastic drop in transmission speed (V).

So far, we have looked qualitatively at how V and $\mathcal{C}_{max}$ are affected by φ and D. To quantitatively explain this relationship, we turn to Eq. (30), where we may use the concepts of destructive and constructive interferences. Equation (30) can be analogous to the well-known phenomenon of wave interference, with the exception that it incorporates Bessel functions instead of amplitudes of interfering waves. The quality of entanglement transmission is determined by the sign of the last term in Eq. (30). In other words, the function $f(\varphi, J, D) = \sin(\varphi)\mathrm{sgn}[J] + D\cos(\varphi)$ in this equation plays a pivotal and meaningful role in establishing the propagation of entanglement through the chain.

In this analysis, we investigate the factors that signify destructive interference in the context of wave interference and can provide a rationale for the occurrence of the minima shown in Fig. 5. Given this matter, it can be asserted that if $f(\varphi, J, D)$ holds the greatest positive magnitude, the requirement for destructive interference is met [in accordance with the negative symbol following it in Eq. (30)]. When $D = 0$ and $J = -1$, $J\sin(\varphi)$ will have the greatest value if $\varphi = -\pi/2$. A decrease in the value of φ will result in a corresponding decrease in this term. Assuming a constant value of J, if D starts to grow, φ must correspondingly approach zero ($\varphi \to 0$) to maximize the values of $f(\varphi, J, D)$. Undoubtedly, this sentence remains accurate even when evaluating the denominator as $\sqrt{1 + D^2}$. Figure 5(a) confirms that when the value of D increases, the minimum of the $\mathcal{C}_{max}$ function occurs at φ values approaching zero.

On the other hand, for constructive interference, which explains the peaks in Fig. 5(a), it can be said that when D is absent, the value of $J\sin(\varphi)$ is greatly influenced by $\varphi = \pi/2$. Consequently, this term becomes large and significant [as indicated by the negative sign in the coefficient
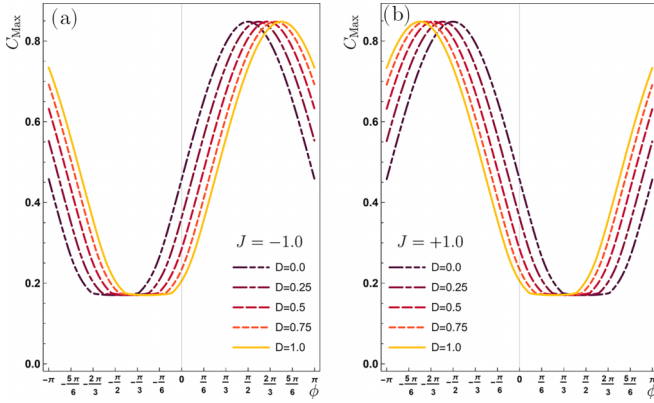
FIG. 5. Maximum concurrence value for (2,3) against φ. Comparing these panels with those of Fig. 3 shows that the lowest entanglement value causes a phase interval during which the speed behaves critically.

in Eq. (30), given $J < 0$]. Conversely, when D increases, φ should approach π for the value of $f(\varphi, J, D)$ to stay big, yet negative, hence amplifying the effects of constructive interference. Figure 5(a) confirms that when the value of D increases, the maximum of the function occurs at φ values approaching π. The contents mentioned here can be generalized for the scenario where $J > 0$, which determines the outcomes of Fig. 5(b). We abstain from delving into the subject matter at this juncture in order to prevent protracted debates.

As previously stated, how c_{max} changes in terms of D completely depends on the value of φ. This statement is also proved in Fig. 5, where raising the value of D leads to drop of c_{max} at $\varphi = 0$. On the other hand, at $\varphi = \pi$, raising D causes an increase in c_{max}.

V. CONCLUSION

Many researchers have focused on the implications of systems like one-dimensional spin chains because of their interest

in the QST traits they exhibit. The QST process, which involves the use of spin structures in entanglement transmission, is just one example of the many exciting avenues that have opened up because of the cooperation between the quantum information community and the field of quantum magnetism. The focus of this study has been on the QST characteristics of the spin-1/2 XX chain associated with a staggered type of DM interaction. The system's initial state that is to be transformed consists of a pair of entangled qubits that, of course, govern by an arbitrary phase, while the other particles are fully nonentangled. The time evolution operator was used to generate the time-dependent quantum state and reduced density matrix for any closest pair of spins We made use of Jordan-Wigner transformation to get a closed form for the system's wave function at time t. Consequently, we looked at the time dependence of the concurrence function (for monitoring entanglement) for every nearest neighbor spaced X apart from the IEP. We found that for a distance X, the time needed for the entanglement crests (t_{max}) to meet a pair site is proportional to X. Using the slope of the $X - t_{max}$ plot, we were able to derive the measurable values of speed at which entanglement spreads. The results demonstrated that higher levels of D lead to faster propagation. Nevertheless, the growth of the speed is not directly proportional to D. We likewise examined the impact of the phase factor (φ) regulating the initial state of the system on the spread of entanglement. It turns out that there are specific values of the phase factor responsible for drastically dropping the entanglement's speed. We have additionally demonstrated the ability to forecast the precise position of these significant declines by employing the principles of wave interference. This attribute is ubiquitous and may be observed for both ferro- and antiferromagnetic-type Heisenberg exchanges. Moreover, entanglement crests that reach any pair, a key factor in determining the value of transmission speed, was shown to be a function of φ as well. The mentioned function reaches its minimum value in the phase interval where the speed profile flattens out.

[1] D. S. Weiss and M. Saffman, Phys. Today **70**(7), 44 (2017).

[2] A. Negretti, P. Treutlein, and T. Calarco, Quantum Info. Proc. **10**, 721 (2011).

[3] J. J. García-Ripoll, P. Zoller, and J. I. Cirac, J. Phys. B: At. Mol. Opt. Phys. **38**, S567 (2005).

[4] J. Benhelm, G. Kirchmair, C. F. Roos, and R. Blatt, Nat. Phys. **4**, 463 (2008).

[5] C. D. Bruzewicz, J. Chiaverini, R. McConnell, and J. M. Sage, Appl. Phys. Rev. **6**, 021314 (2019).

[6] B. P. Lanyon, P. Jurcevic, M. Zwerger, C. Hempel, E. A. Martinez, W. Dür, H. J. Briegel, R. Blatt, and C. F. Roos, Phys. Rev. Lett. **111**, 210501 (2013).

[7] J. You and F. Nori, Phys. Today **58**(11), 42 (2005).

[8] E. Jeffrey, D. Sank, J. Y. Mutus, T. C. White, J. Kelly, R. Barends, Y. Chen, Z. Chen, B. Chiaro, A. Dunsworth, A. Megrant, P. J. J. OMalley, C. Neill, P. Roushan, A. Vainsencher,

J. Wenner, A. N. Cleland, and J. M. Martinis, Phys. Rev. Lett. **112**, 190504 (2014).

[9] T. Brecht, W. Pfaff, C. Wang, Y. Chu, L. Frunzio, M. H. Devoret, and R. J. Schoelkopf, npj Quantum Inf. **2**, 16002 (2016).

[10] J. M. Gambetta, J. M. Chow, and M. Steffen, npj Quantum Inf. **3**, 2 (2017).

[11] X. Liu, X. Yao, H. Wang, H. Li, Z. Wang, L. You, Y. Huang, and W. Zhang, Appl. Phys. Lett. **114**, 141104 (2019).

[12] M. Huo, J. Qin, J. Cheng, Z. Yan, Z. Qin, X. Su, X. Jia, C. Xie, and K. Peng, Sci. Adv. **4**, eaas9401 (2018).

[13] Y.-A. Chen, Q. Zhang, T.-Y. Chen, W.-Q. Cai, S.-K. Liao, J. Zhang, K. Chen, J. Yin, J.-G. Ren, Z. Chen, S.-L. Han, Q. Yu, K. Liang, F. Zhou, X. Yuan, M.-S. Zhao, T.-Y. Wang, X. Jiang, L. Zhang, W.-Y. Liu *et al.*, Nature (London) **589**, 214 (2021).

[14] J. S. Canseco and A. Valdés-Hernández, J. Phys. A: Math. Theor. **55**, 405301 (2022).

[15] A. Bienfait, K. J. Satzinger, Y. Zhong, H.-S. Chang, M.-H. Chou, C. R. Conner, É. Dumur, J. Grebel, G. A. Peairs, R. G. Povey, and A. N. Cleland, Science **364**, 368 (2019).

[16] B. Vermersch, P.-O. Guimond, H. Pichler, and P. Zoller, Phys. Rev. Lett. **118**, 133601 (2017).

[17] Y. He, Y.-M. He, Y.-J. Wei, X. Jiang, K. Chen, C.-Y. Lu, J.-W. Pan, C. Schneider, M. Kamp, and S. Höfling, Phys. Rev. Lett. **119**, 060501 (2017).

[18] N. Maring, P. Farrera, K. Kutluer, M. Mazzera, G. Heinze, and H. de Riedmatten, Nature (London) **551**, 485 (2017).

[19] E. A. Sete and H. Eleuch, Phys. Rev. A **91**, 032309 (2015).

[20] Y. P. Kandel, H. Qiao, S. Fallahi, G. C. Gardner, M. J. Manfra, and J. M. Nichol, Nat. Commun. **12**, 2156 (2021).

[21] A. Zwick, G. A. Alvarez, J. Stolze, and O. Osenda, Phys. Rev. A **84**, 022311 (2011).

[22] T. Shi, Y. Li, Z. Song, and C.-P. Sun, Phys. Rev. A **71**, 032309 (2005).

[23] A. Juozapavičius, L. Urba, S. Caprara, and A. Rosengren, Phys. Rev. B **60**, 14771 (1999).

[24] J. E. Bunder and R. H. McKenzie, Phys. Rev. B **60**, 344 (1999).

[25] F.-W. Ma, S.-X. Liu, and X.-M. Kong, Phys. Rev. A **83**, 062309 (2011).

[26] S. Furukawa, M. Sato, S. Onoda, and A. Furusaki, Phys. Rev. B **86**, 094417 (2012).

[27] P. Laurell, G. Alvarez, and E. Dagotto, Phys. Rev. B **107**, 104414 (2023).

[28] M. Motamedifar, S. Mahdavifar, and S. F. Shayesteh, J. Supercond. Novel Magn. **24**, 769 (2011).

[29] M. Motamedifar, S. Mahdavifar, and S. Farjami Shayesteh, Eur. Phys. J. B **83**, 181 (2011).

[30] M. Motamedifar, S. Mahdavifar, S. F. Shayesteh, and S. Nemati, Phys. Scr. **88**, 015003 (2013).

[31] S. Bose, Phys. Rev. Lett. **91**, 207901 (2003).

[32] M. Motamedifar, M. Abbasi, M. Golshani, A.-B. Mohamed, and A. H. Homid, Eur. Phys. J. Plus **139**, 18 (2024).

[33] E. Dorrani, H. Safari, and M. Motamedifar, Phys. Scr. **95**, 095402 (2020).

[34] M. Motamedifar, Physica A **568**, 125745 (2021).

[35] S. Shahsavari, M. Motamedifar, and H. Safari, Phys. Scr. **95**, 015102 (2020).

[36] X. Shi, H. Yuan, X. Mao, Y. Ma, and H. Q. Zhao, Phys. Rev. A **95**, 052332 (2017).

[37] I. Dzyaloshinsky, J. Phys. Chem. Solids **4**, 241 (1958).

[38] T. Moriya, Phys. Rev. **120**, 91 (1960).

[39] K. V. Kavokin, Phys. Rev. B **64**, 075305 (2001).

[40] J. Fransson, J. Ren, and J.-X. Zhu, Phys. Rev. Lett. **113**, 257201 (2014).

[41] S. Roy, T. Chanda, T. Das, D. Sadhukhan, A. SenDe, and U. Sen, Phys. Rev. B **99**, 064422 (2019).

[42] M. E. S. Nunes, E. de Mello Silva, P. H. L. Martins, J. A. Plascak, and J. Florencio, Phys. Rev. E **98**, 042124 (2018).

[43] B.-Q. Liu, B. Shao, J.-G. Li, J. Zou, and L.-A. Wu, Phys. Rev. A **83**, 052112 (2011).

[44] N. Avalishvili, G. I. Japaridze, and G. L. Rossini, Phys. Rev. B **99**, 205159 (2019).

[45] N. Avalishvili, B. Beradze, and G. I. Japaridze, Eur. Phys. J. B **92**, 262 (2019).

[46] G. I. Japaridze, H. Cheraghi, and S. Mahdavifar, Phys. Rev. E **104**, 014134 (2021).

[47] M. Motamedifar, F. Sadeghi, and M. Golshani, Sci. Rep. **13**, 2932 (2023).

[48] B. Li, Y. Cao, Y.-H. Li, W.-Q. Cai, W.-Y. Liu, J.-G. Ren, S.-K. Liao, H.-N. Wu, S.-L. Li, L. Li, N.-L. Liu, C.-Y. Lu, J. Yin, Y.-A. Chen, C.-Z. Peng, and J.-W. Pan, Phys. Rev. Lett. **128**, 170501 (2022).

[49] Y. Lee, H. Yamasaki, and S. Lee, Phys. Rev. A **103**, 062613 (2021).

[50] M. Motamedifar, Quantum Info. Proc. **16**, 162 (2017).

[51] A.-B. Mohamed, A. Rahman, and F. Aldosari, Alexandria Eng. J. **66**, 861 (2023).

[52] M. Motamedifar and M. Golshani, Quantum Info. Proc. **18**, 181 (2019).

[53] G. Arfken, H. Weber, and F. Harris, *Mathematical Methods for Physicists: A Comprehensive Guide* (Elsevier Science, New York, 2013).

[54] C. H. Bennett, D. P. DiVincenzo, J. A. Smolin, and W. K. Wootters, Phys. Rev. A **54**, 3824 (1996).

[55] S. Heusler, W. Dür, M. S. Ubben, and A. Hartmann, J. Phys. A: Math. Theor. **55**, 404006 (2022).

[56] S. A. Hill and W. K. Wootters, Phys. Rev. Lett. **78**, 5022 (1997).

[57] W. K. Wootters, Phys. Rev. Lett. **80**, 2245 (1998).

[58] V. Coffman, J. Kundu, and W. K. Wootters, Phys. Rev. A **61**, 052306 (2000).